This is an pre-print of the paper published by Elsevier in Applied Thermal Engineering 106 (2016) 1337–1344
kris@kubiak.co.uk
http://dx.doi.org/10.1016/j.applthermaleng.2016.06.128

Dropwise condensation heat transfer process optimisation on superhydrophobic surfaces using a multi-disciplinary approach

Z. Khatir [a]*, K.J. Kubiak[b], P.K. Jimack[c], T.G. Mathia[d]

[c] University of Leeds, School of Chemical & Process Engineering, Leeds LS2 9JT, United Kingdom
[b] University of Huddersfield, School of Computing & Engineering, Huddersfield HD1 3DH, United Kingdom
[c] University of Leeds, School of Computing, Leeds LS2 9JT, United Kingdom
[d] Ecole Centrale de Lyon (LTDS), CNRS UMR5513, 69134 Ecully, France

kris@kubiak.co.uk

Abstract

Dropwise condensation has superior heat transfer efficiency than filmwise condensation; however condensate evacuation from the surface still remains a significant technological challenge. The process of droplets jumping, against adhesive forces, from a solid surface upon coalescence has been studied using both experimental and Computational Fluid Dynamics (CFD) analysis. Both Lattice Boltzmann (LBM) and Volume of Fluid (VOF) methods have been used to evaluate different kinematic conditions of coalescence inducing a jump velocity. In this paper, an optimisation framework for superhydrophobic surface designs is presented which uses experimentally verified high fidelity CFD analyses to identify optimal combinations of design features which maximise desirable characteristics such as the vertical velocity of the merged jumping droplet from the surface and energy efficiency. A Radial Basis Function (RBF)-based surrogate modelling approach using design of experiment (DOE) technique was used to establish near-optimal initial process parameters around which to focus the study. This multidisciplinary approach allows us to evaluate the jumping phenomenon for superhydrophobic surfaces for which several input parameters may be varied, so as to improve the heat transfer exchange rate on the surface during condensation. Reliable conditions were found to occur for droplets within initial radius range of r=20-40 μm and static contact angle θs~160º. Moreover, the jumping phenomenon was observed for droplets with initial radius of up to 500 μm. Lastly, our study also reveals that a critical contact angle for droplets to jump upon coalescence is θ_c~140º.

Keywords Condensation heat transfer, Super-hydrophobic surface, Jumping droplets velocity, Multi-disciplinary optimisation.

Nomenclature

Abbreviation

CFD	Computational fluid dynamics
DOE	Design of experiment
GA	Genetic algorithm
LB(M)	Laticce Boltzmann (method)
RBF	Radial basis function
VOF	Volume of fluid
2D	Two dimensional
3D	Three dimensional

Symbols

This is an pre-print of the paper published by Elsevier in Applied Thermal Engineering 106 (2016) 1337–1344
kris@kubiak.co.uk
http://dx.doi.org/10.1016/j.applthermaleng.2016.06.128

A	Surface area [m^2]
c_p	Specific heat capacity [J/(kg K)]
g	Gravity [m/s^2]
m	Mass [kg]
P	Pressure [Pa]
Q	Heat energy [J]
q	Heat flux [W/m2]
r	Droplet radius [m]
r^3	Radial basis function
T	Temperature [K]
t	Time [s]
$\vec{v}$	Velocity [m/s]
$\bar{v}$	Mass-averaged *y*-velocity v_y [m/s]
$\bar{v}_j$	Jumping velocity [m/s]
w	Weighting function
α	Phase fraction, $0 \leq \alpha \leq 1$ [-]
ρ	Density [kg/m^3]
μ	Dynamic viscosity [Pa.s]
σ	Surface tension [N/m]
θ	Contact angle [^{o}]

Subscript

c	Critical angle
co	Compression velocity
g	Gas
i	Index i
j	Jumping
l	Liquid
s	Static

1 Introduction

Drop-wise condensation processes, where condensation occurs through small droplets on a solid surface, has been demonstrated to significantly improve heat transfer rates in comparison to film-wise condensation (where a whole surface is covered by a thin film of liquid) [1, 2]. Drop-wise condensation usually takes place on hydrophobic or super-hydrophobic surfaces as demonstrated by Boreyko and Chen [3]. One of the main technological challenges is to create such a surface, so as to allow condensation and evacuation of the droplets to take place in a continuous manner. Droplet coalescence is a complex physical phenomenon and optimisation of kinematic conditions leading to surface dewetting and jumping of droplets is of paramount importance for processes like heat transfer, de-icing, atmospheric water harvesting or dehumidification [4-6]. Dropwise condensation heat transfer performance can be enhanced by allowing condensed droplets to be removed rapidly from the surface to minimize the thermal barrier [7]. Recently, researchers showed that super-hydrophobic surfaces provide a higher mobility of condensates, which may enhance the heat transfer performance [1-7]. Coalescence-induced jumping phenomena occur on superhydrophobic surfaces but within a small range of initial droplet radii. Recent interest in these phenomena has led to the influence of the droplets radii on the resulting jumping velocity to be explored [3, 8-12]. However, previous analysis on coalescence-induced jumping droplets focused only a limited range of contact angles and droplet radius [10-12]. While Liu *et al*. [12] assumed only the contact angle of 180^o; Cheng *et al.* [13] proposed a wider range in their numerical investigations. In this study we investigate such jumping phenomena both experimentally and numerically. We undertake

This is an pre-print of the paper published by Elsevier in Applied Thermal Engineering 106 (2016) 1337–1344
kris@kubiak.co.uk
http://dx.doi.org/10.1016/j.applthermaleng.2016.06.128

experimental analysis for larger droplets, in the range of 400-500μm, and we develop numerical models to explore the effects of variation in initial droplet radius and the static contact angle in the ranges 30-500μm and 130-180^o respectively. We also establish a range of conditions where jumping upon coalescence can take place through a formal optimization framework.

In the following section, we describe both the experimental and the numerical methods that have been developed to undertake this study, as well as providing an overview of the optimization strategy that is used to investigate conditions for which the heat transfer may be maximized. Section 3 then presents typical experimental and computational results which are verified against others appearing in the literature and shown to provide good validation of our numerical simulations. This, in turn, allows us to seek optimal parameter regimes for heat transfer based upon coalescence-induced jumping. The paper ends with some brief conclusions.

2 Materials and methods

In this study experimental analysis of droplet jumping coalescence is carried out to develop and validate two numerical models: a 2D Lattice Boltzmann Method (LBM) and 3D Volume of Fluid (VOF) models.

2.1 Experimental velocity measurement

For the physical experiments, the superhydrophobic surface has been prepared on copper alloy UNS C17000 (sample size 10x10x10mm) by covering the surface with a thin layer of a paraffin film and subsequently by a monolayer of hydrophobic fumed silica particles. The prepared specimen was then heated to 50ºC to create a bond between the silica and paraffin films. Any excess silica powder was cleaned from the surface by a pressurised air jet. Such prepared surface is superhydrophobic with a measured static contact angle of θ_s=157±2º (Fig.1).

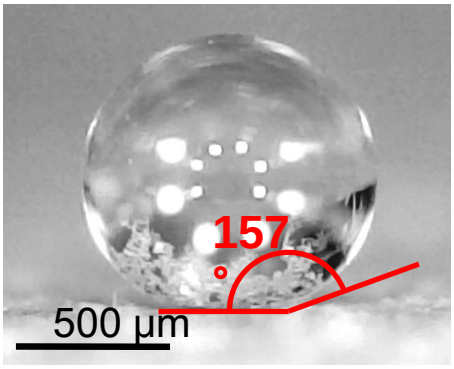

Figure 1: Contact angle measurement of water droplet on a superhydrophobic surface prepared on copper alloy.

To extend the range of experimentally explored conditions a number of water droplets sizes were used which experience a jumping phenomenon upon coalescence: the initial radii being from 100 to 515μm. A shadowgraph technique was used to measure the droplet size with a diffused light source. Horizontal and vertical diameters of the droplets were measured and an average value was calculated. Calibration was undertaken using 1mm radius stainless steel ball. For larger droplet cases, the droplets were formed from two smaller droplets of quasi-identical size which were carefully deposited on the superhydrophobic surface using a micro-pipette (0.2-2μl). These droplets were initially deposited in very close proximity so that even small vibrations or spreading lead to droplet movement and coalescence. For the smaller droplet cases, in the range of 100-300 μm, a mist of distilled water was created using a manual atomiser and was sprayed onto the superhydrophobic surface. This lead to the formation of droplets, followed by coalescence of neighbours and finally to

This is an pre-print of the paper published by Elsevier in Applied Thermal Engineering 106 (2016) 1337–1344
kris@kubiak.co.uk
http://dx.doi.org/10.1016/j.applthermaleng.2016.06.128

droplets jumping phenomenon. Several repetitions of this procedure allowed us to select a number of droplet jumping events to cover a wide range of droplet sizes. The process was recorded with high speed Mikrotron MotionBlitz EoSence CL camera, with a frame rate of 1200 fps. Examples of droplets with initial radius of 515 μm are presented in Fig. 6 The initial droplet velocities were measured by tracing the droplets' vertical position as a function of a time, and the slope of the resulting curve at the point when a droplet leaves the surface is taken as the initial jump velocity of that droplet. However, due to droplet oscillations, the vertical position of the droplet is calculated as the midpoint between the top and bottom droplet interface. This methodology was also used to calculate the initial droplet velocity in the numerical simulations described below.

2.2 Lattice Boltzmann method

Our LB solver is based on the Shan-Chen [14] multiphase model, with wetting boundary conditions based upon the adhesion force described by Sukop and Thorne [15]. In particular, we use the OpenLBMflow code [16], with a modified adhesion term for wettability. The main advantage of the lattice Boltzmann method is that the interface between light and heavy fluids is diffuse, and the position of interface is computed as a result of the simulation. In particular, this approach does not require interface tracking or reconstruction. However, the modelled fluid can change phase and as it can be noticed in Fig. 7 the air initially trapped between coalescing droplets compresses and change to a heavy phase (water). Unless otherwise stated, the following parameters were used in all of lattice Boltzmann simulations described in this work: G= -6, ρ_L=0.0734 ρ_H=2.65, τ=0.54, $\delta x=2.5\times10^{-6}$m, $\delta t=2.86\times10^{-7}$s. These parameters correspond to dynamic conditions of water with surface tension σ=0.0727 N/m and dynamic viscosity $\mu=4.3\times10^{-3}$ Pa.s. A detailed description of this lattice Boltzmann solver may be found in [17].

2.3 Volume of Fluid (VOF) Method

For our finite volume simulations the two-phase interFoam solver [18] from the OpenFOAM open source CFD software tool [19] was chosen. This solver includes automatic interface tracking and mass conservation. Unlike other numerical techniques [20] dealing with complex wall-boundary flow systems interFoam uses a VOF [21] approach modified with the introduction of an additional term in the volume fraction equation, to obtain interface compression by means of a tuneable parameter as detailed in [22].

In the conventional volume-of-fluid (VOF) method, the transport equation for an indicator function, representing the volume fraction of one phase, is solved simultaneously with the continuity and momentum equations:

$$\rho\left(\frac{\partial\vec{v}}{\partial t}+\ \vec{v}.\nabla\vec{v}\right)=\ \nabla P+\ \nabla(\mu(\nabla.\vec{v}+\nabla.\vec{v}^{T}))+\rho g \qquad (1)$$

$$\nabla.\vec{v}=0 \qquad (2)$$

$$\left(\frac{\partial\alpha}{\partial t}+\ \vec{v}.\nabla\alpha\right)=0 \qquad (3)$$

where $\vec{v}$ represents the velocity field shared by the two fluids throughout the flow domain, α is the phase fraction, μ the viscosity, ρ the density, P the pressure and g the gravity. The phase fraction α can take values within the range $0 \leq \alpha \leq 1$, with the values of zero and one corresponding to regions accommodating only one phase, e.g. α = 0 for gas, α = 1 for liquid. Accordingly, gradients of the phase fraction are encountered only in the region of the interface as represented in Fig. 2.

This is an pre-print of the paper published by Elsevier in Applied Thermal Engineering 106 (2016) 1337–1344
kris@kubiak.co.uk
http://dx.doi.org/10.1016/j.applthermaleng.2016.06.128

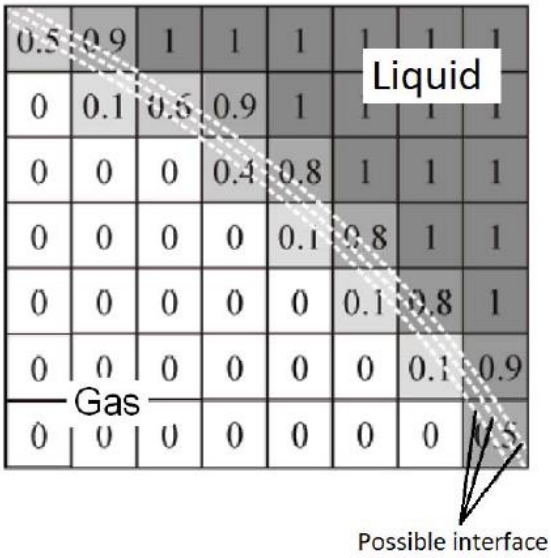

Figure 2: The VOF method indicating values of the phase fraction α: $\alpha = 0$ for gas, $\alpha = 1$ for liquid and $0 \leq \alpha \leq 1$ for the interface.

Two immiscible fluids are considered as one effective fluid throughout the domain, the physical properties of which are calculated as weighted averages based on the distribution of the liquid volume fraction,:

$$\rho = \rho_l \alpha + \rho_g (1 - \alpha) \quad (4)$$

$$\mu = \mu_l \alpha + \mu_g (1 - \alpha) \quad (5)$$

where ρ_l and ρ_g are the liquid and gas densities, whereas μ_l and μ_g are the liquid and gas viscosities respectively.

In the present study a modified approach similar to the one proposed in [23] is used, which is formulated in the interFoam flow solver [18], relying on a two-fluid formulation of the conventional volume-of-fluid model in the framework of finite volume method.
In this model an additional convective term originating from modelling the velocity in terms of weighted average of the corresponding liquid and gas velocities is introduced into the transport equation for phase fraction, providing a sharper interface resolution. The model makes use of the two-fluid Eulerian model for two-phase flow, where phase fraction equations are solved separately for each individual phase (see [24]); hence the equations for each of the phase fractions can be expressed as

$$\frac{\partial \alpha}{\partial t} + \vec{v}_l \cdot \nabla \alpha = 0 \quad (6)$$

$$\frac{\partial (1-\alpha)}{\partial t} + \vec{v}_g \cdot \nabla (1 - \alpha) = 0 \quad (7)$$

where the subscripts l and g denote the liquid and gaseous phase, respectively. Assuming that the contributions of the liquid and gas velocities to the evolution of the free surface are proportional to the corresponding phase fraction, and defining the velocity of the effective fluid in a VOF model as a weighted average

$$\vec{u} = \alpha \vec{v}_l + (1 - \alpha) \vec{v}_g \quad (8)$$

Equation 6 can be rearranged and used as an evolution equation for the phase fraction α,

This is an pre-print of the paper published by Elsevier in Applied Thermal Engineering 106 (2016) 1337–1344
kris@kubiak.co.uk
http://dx.doi.org/10.1016/j.applthermaleng.2016.06.128

$$\frac{\partial \alpha}{\partial t} + \vec{v} \,.\nabla\alpha + \vec{v}_{co} \,.\nabla(\alpha(1-\alpha)) = 0 \qquad (9)$$

where $\vec{v}_{co} = \vec{v}_l - \vec{v}_g$ is the vector of relative velocity, designated as the "compression velocity".

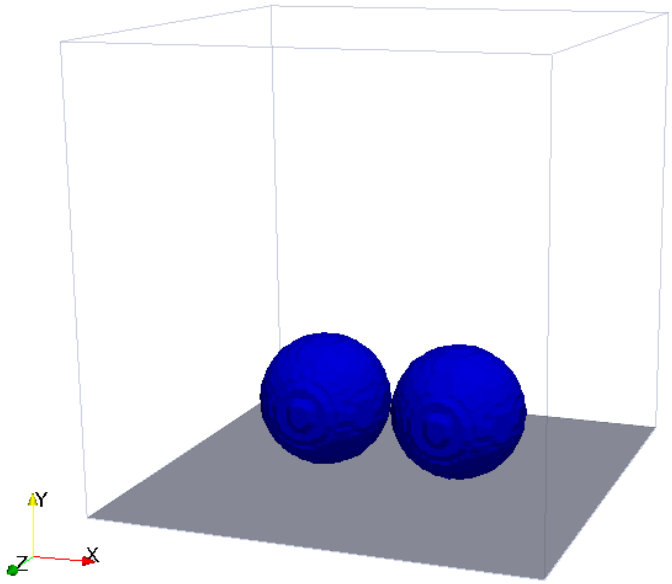

Figure 3: 3D VOF flow domain *D* emphasising two droplets on the functional surface.

The VOF domain consists of the $[0, 2600\mu m]^3$ block discretised with around 1.3M cuboid elements as indicated in Figure 3 with: (i) no-slip imposed on the bottom, left and right walls for velocity, (ii) zero dynamic pressure and (iii) zero gradient on left and right walls with constant static angle equals to θ_s on the bottom wall for phase fraction.

The VOF numerical methodology is validated and tested against the results published by Liu *et al*. [12]. The validation mainly focuses on the evaluation on the maximum velocity of merged droplet upon the coalescence of two symmetrical droplets with initial radius r = 75μm and static contact angle $\theta_s = 180^\circ$. This was the only contact angle considered in [12].
The resulting process of the 3D coalescence is depicted in Figure 4 and is in agreement with that one of Liu *et al*. [12]. After the coalescence is originated by the overlapping interfaces, a liquid bridge develops upon coalescence with an expanding bridge reaching the surface at around 0.00007s, at which point the merged droplet experiences an upward motion. The functional surface counteracts the impingement of the liquid bridge, forcing a portion of the downward-moving mass towards the sides, leading to a maximum deformation in the *x* direction at 0.00009s. The upward force from the surface culminates at 0.000175s, beyond which the apparent contact area between the merged drop and the substrate gradually reduces towards zero at 0.000255s, the point of departure. The launched droplet continues to oscillate while maintaining the upward motion.

For the coalescence of two symmetric identical droplets, similarly to Liu *Et al*. [12] and F. Raees *Et al*. [25] we define the instantaneous velocity of the merged droplet $\bar{v}$ by mass-averaging the *y* component of velocity over the entire droplet,

$$\bar{v} = \frac{\int \alpha \rho_l \, v_y \, dD}{\int \alpha \rho_l \, dD} \qquad (10)$$

This is an pre-print of the paper published by Elsevier in Applied Thermal Engineering 106 (2016) 1337–1344
kris@kubiak.co.uk
http://dx.doi.org/10.1016/j.applthermaleng.2016.06.128

where D represents the entire computational domain and y is the vertical direction perpendicular to the functional surface as displayed in Figure 3.

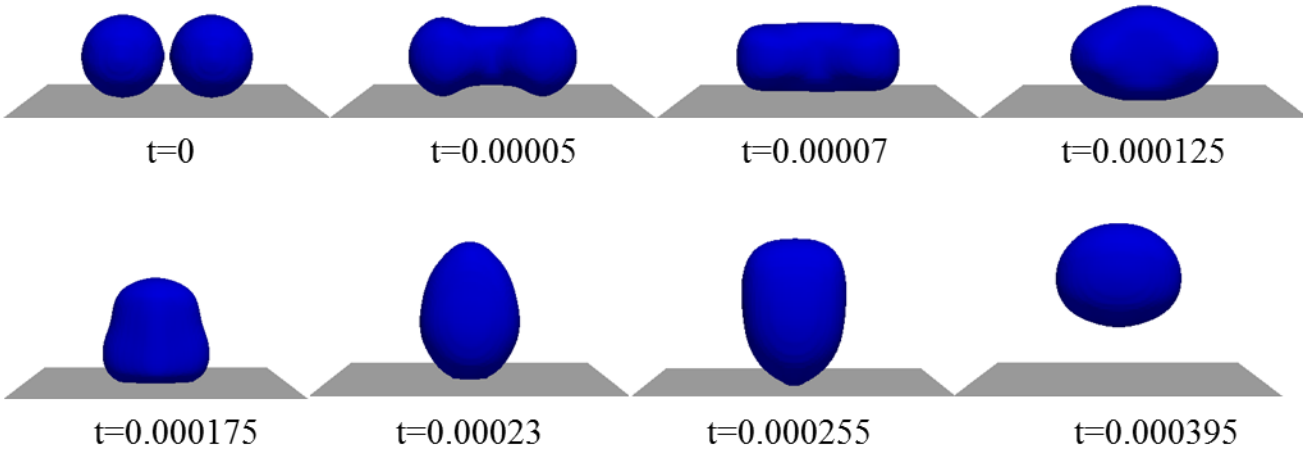

Figure 4: Time sequence of the 3D coalescence of two droplets (*x*-*y* view) with initial radius r =75μm and static angle θ_s = 180°. The isosurface α=0.5 is displayed.

A further illustration of the jumping process in the above Figure 4 is shown in Figure 5 where the temporal evolution of the droplet velocity defined in (10). As identified by Liu *Et al*. [12] and based on these figures, the jumping process upon coalescence can be approximately divided into four stages: (I) expansion of the liquid bridge between the coalescing droplets, till approximately 0.00007s; (II) acceleration of the merged droplet on the surface, eventually reaching a maximum velocity at 0.00023s; (III) detachment of the merged droplet from the surface, till a complete departure at 0.000255s; and (IV) deceleration of the departed drop in air, where the oscillating drop relaxes towards the ultimate equilibrium shape of a sphere.

The jumping velocity $\bar{v}_j$ is extracted from the curve and is found to be 0.210 m/s and is in very good agreement with the value 0.211 m/s found Liu *Et al*. [12].

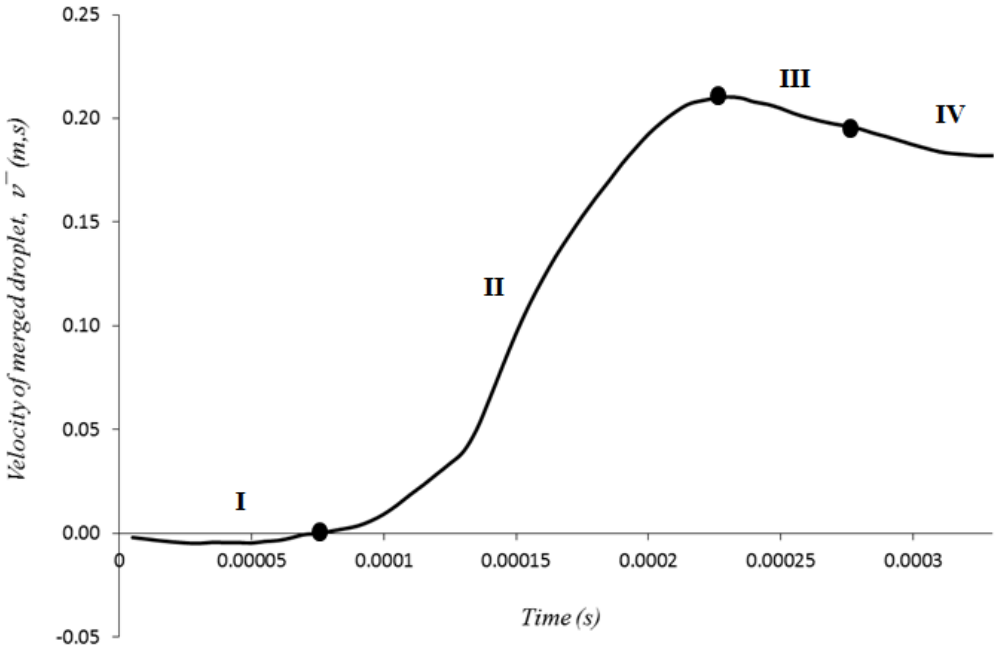

Figure 5: Evolution of the instantaneous droplet velocity during the jumping process of Fig. 4.

This is an pre-print of the paper published by Elsevier in Applied Thermal Engineering 106 (2016) 1337–1344
kris@kubiak.co.uk
http://dx.doi.org/10.1016/j.applthermaleng.2016.06.128

As identified by Liu *Et al*. [12], the $\bar{v}(t)$ curve can be divided into four regimes: I, expansion of the liquid bridge in the air; II, acceleration of the merged drop on the substrate; III, departure of the merged drop from the substrate; and IV, deceleration of the departed drop in the air.

2.4 Heat transfer model

Note that the fluid models described above assume that the flow is isothermal. This approximation is based upon the assumption that the heat transfer between the wall and the droplets is sufficiently rapid that it occurs well before coalescence has completed. Whilst it is likely that this assumption will only be valid for sufficiently small droplets we do not investigate the precise range of validity in this work.

Under the assumption that: (i) the coalescence process of two identical spherical droplets with radius r results in a droplet of radius $\sqrt[3]{2}r$; (ii) there is a temperature difference ΔT between the droplets and the functional surface; (iii) rapid removal of the heated resulting jumping droplets of radius $\sqrt[3]{2}r$ from the wall surface upon coalescence is taking place to reduce the thermal barrier effects; the heat Q between the droplets and the functional surface can hence be evaluated as

$$Q = m\, c_p\, \Delta T \tag{11}$$

where $m = \rho_l \frac{8\pi}{3r^3}$ with ρ_l denoting the liquid density and c_p is the specific heat.
The heat flux q is then determined by:

$$q = Q/A \tag{12}$$

and A represents the surface area.

2.5 Optimisation strategy

The jumping velocity $\bar{v}_j$ is parametrised in terms of the two design variables, namely the droplet radius r and the contact angle θ. A multi-design optimisation processes are carried out whose goals are to: (i) maximise the jumping velocity $\bar{v}_j$ and (ii) maximise both $\bar{v}_j$ and the heat flux q. Due to the computational requirements of the 3D VOF CFD and the experimental analyses, a surrogate modelling approach is adopted for the optimisation study, a methodology that has been successfully applied by the authors for a range of engineering applications, e.g. the design optimisation of commercial ovens [26-28]. A Design of experiments (DOE) approach based on 2D LBM is used to generate 67 points uniformly spread within the design space $(r, \theta) \in [30, 500] \times [130, 180]$. Note that our computational results in section 3.2 below indicate a sufficiently strong correlation between the 2D LBM predictions and the (much more expensive) full 3D VOF predictions to justify this approach.

A Radial Basis Function (RBF) method [29], shown to be an effective design tool for industrial applications such as combustion systems [30] for instance, is employed to build the surrogate models of $\bar{v}_j$, where a cubic radial power function is used to determine the weighting of points in the regression analysis at each point:

$$w_i = r_i^3 \tag{12}$$

The RBF-based surrogate models for the jumping velocity $\bar{v}_j$ and heat flux, q are built by carrying out 2D LBM CFD calculations and solutions of Eq. (12) respectively at each of the DOE points and

This is an pre-print of the paper published by Elsevier in Applied Thermal Engineering 106 (2016) 1337–1344
kris@kubiak.co.uk
http://dx.doi.org/10.1016/j.applthermaleng.2016.06.128

using these values to build surrogate models of their dependence on the design variables throughout the design space.

3 Results and discussion

3.1 Experimental results

Droplets jumping upon coalescence are of particular interest for number of engineering applications, however the physical conditions for which coalescence will lead to dewetting of a surface are limited to superhydrophobic surfaces with low contact angle hysteresis. Usually, superhydrophobic surfaces will have high roughness and droplets will remain in the so-called Cassie-Baxter state where only peaks of roughness morphology will be in contact with water. This state significantly facilitates the dewetting process after coalescence however it also renders the surface to appear more soft than for a flat surface of the same material. Consequently, the experimentally observed jumping velocity will usually be slightly lower than the theoretical and numerically simulated estimates. Our experimental results show jumping velocities from 0.14 m/s for droplets of r=96.5 μm down to 0.039 m/s for droplets of r=515 μm. An example of a droplet jumping after coalescence is presented in Fig. 6. Note that these experimental data are in good agreement with previously published results [3]. The experimental data were used also to validate results of the numerical 2D and 3D models.

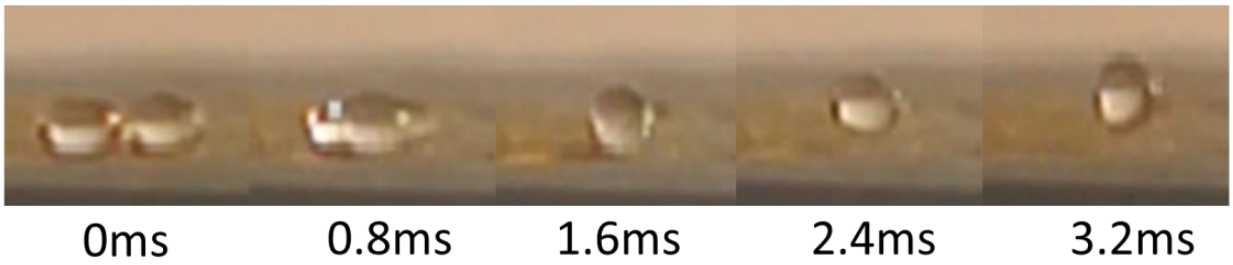

Figure 6: Experimental validation of jumping phenomenon on superhydrophobic surface, droplet with initial radius 515 μm jumping upon coalescence, droplet velocity $\bar{v}_j$ =0.039 m/s.

3.2 LBM and VOF results

As described above, the droplets' coalescence and jumping phenomena have been modelled numerically using both 2D LB (Fig. 7) and 3D VOF (Fig. 8) methods. Analysing the results of this numerical modelling, we believe that the primary jumping phenomenon can be explained as a dynamic process where the diameter of resulting droplet, following coalescence, is larger than the diameters of the initial droplets.

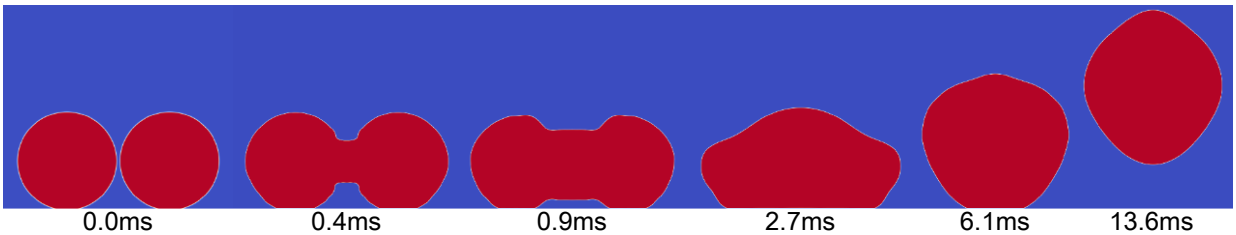

Figure 7: Results of 2D LB modelling of droplet coalescence and jumping phenomenon, initial droplet radius 405 μm and droplet velocity $\bar{v}_j$ =0.064 m/s.

Kinetic momentum created initially by the coalescing droplets acts in horizontal direction, and deforms the interface, but the droplet can only escape upwards due to the close proximity of the solid wall (see the change of shape between 2.7ms and 6.1ms in Figure 7, and the change of shape between 0.8ms and 1.6ms in Figure 8 – note that the different time-scales is explained by the

This is an pre-print of the paper published by Elsevier in Applied Thermal Engineering 106 (2016) 1337–1344
kris@kubiak.co.uk
http://dx.doi.org/10.1016/j.applthermaleng.2016.06.128

difference between 2D and 3D droplets. If the resulting vertical force, acting on the combined drop, is sufficient to overcome the adhesion forces between the surface and the droplet, the droplet will jump away from the surface. Viscous dissipation of the fluid will also take place. Further analysis concentrated on establishing necessary kinematic conditions for this jumping phenomenon to occur. A Design of Experiment approach was followed, with the initial droplet radius (r) and the static contact angle (θ_s) of the surface being analysed through 2D numerical simulations. The estimated surface response obtained from this analysis is presented in Figure 11.

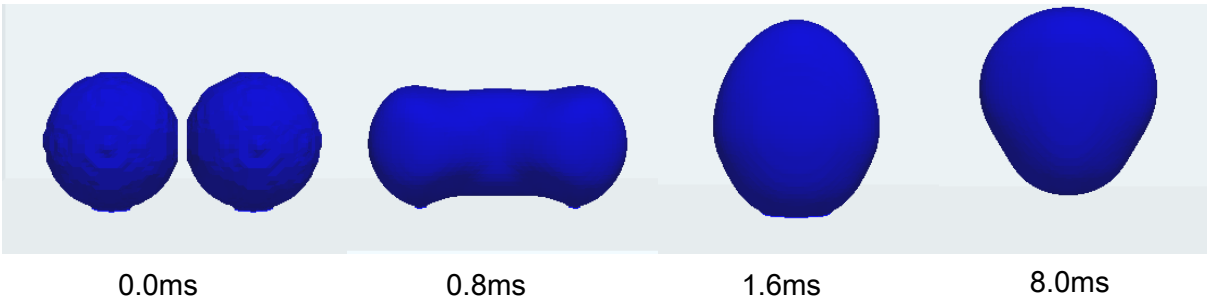

Figure 8: Results of 3D VOF modelling of droplet coalescence and jumping phenomenon, initial droplet radius 405 µm and droplet velocity U=0.082 m/s.

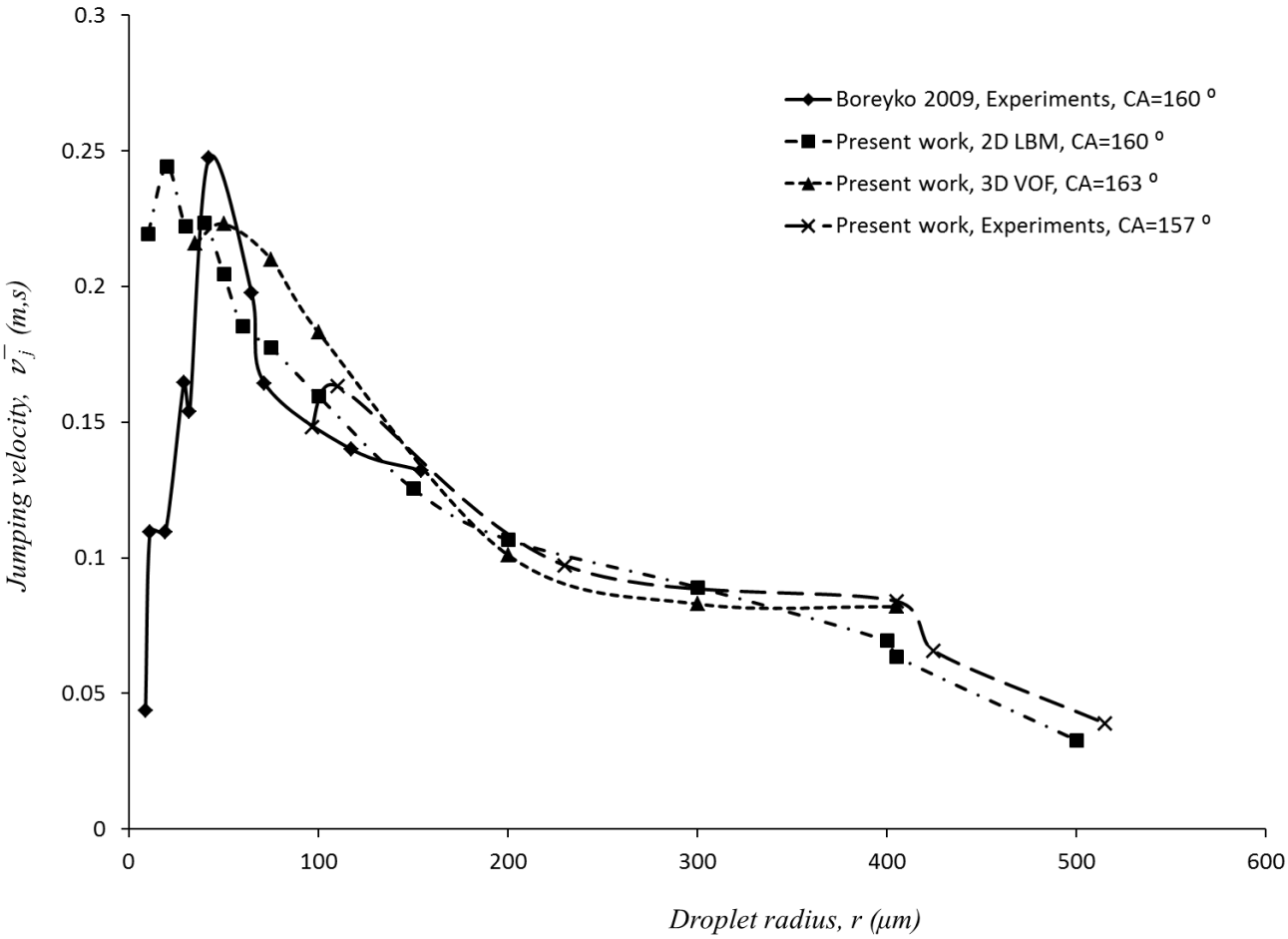

Figure 9: Comparison of numerical simulations and experimental analysis together with the experimental data from Boreyko & Chen [3].

This is an pre-print of the paper published by Elsevier in Applied Thermal Engineering 106 (2016) 1337–1344
kris@kubiak.co.uk
http://dx.doi.org/10.1016/j.applthermaleng.2016.06.128

It may be noted that the jumping velocity is higher for more hydrophobic surfaces. This may be explained by the fact that the contact area between the merged droplet and the surface is smaller; therefore less energy is required to dewet the surface. Despite the expected advantage of more superhydrophobic surfaces, it is difficult to fabricate a long-lasting surface with static contact angle significantly above 160º. Hence, due to our desire for experimental validation, we focused our remaining simulations on surface with θ_s=160º. Analysing the initial droplet radius we conclude that the jumping velocity increases for smaller droplets with initial radius of about 30μm (Figure 11), however for smaller droplets (<20μm) the jump velocity follows experimental observations and decreases (see Figure 9, LB curve).

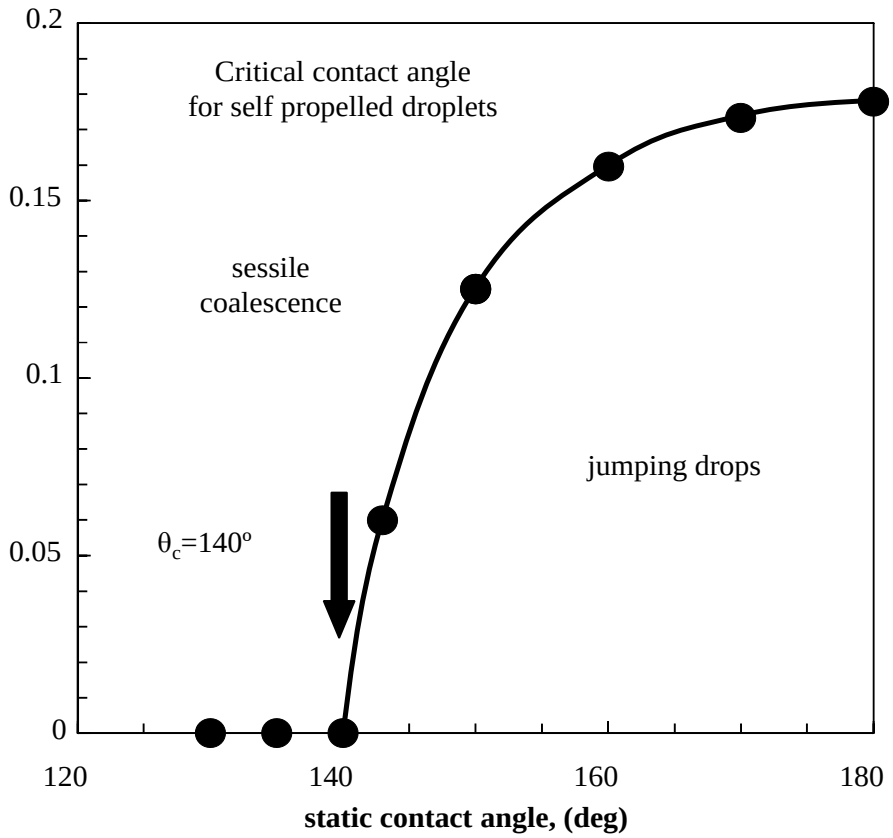

Figure 10: Influence of the static contact angle on the droplet jumping velocity, and determination of critical contact angle for jumping phenomenon (θ_c=140º) (after Khatir & Kubiak [31]).

Figure 10 shows the influence of the static contact angle on the jumping velocity, and a critical value of the static contact angle has been obtained (θ_c=140º) for droplets with initial 2D radius of 100 μm. Jumping occurs for all values of θ between 140º and 180º. However, for a surface with static contact angle θ=160º, the jumping velocity is already 90% of the jumping velocity for θ=180º. A wider selection of numerical results is presented in Figure 9, which shows very good agreement with experimental values across a wide range of initial droplet radii from 20μm up to 500μm. Overall, the numerical methods developed in this study appear to show reliable predictions. So far maximum jumping velocity reported in the literature from numerical simulations [12] and experimental analysis [3] is in the region of 0.25 m/s, which is consistent with our results presented in this paper. Note that fewer computational results for the 3D simulations by the VOF method. These results are considerable more computationally demanding, however they demonstrate very good agreement with experimental data and with data published by Liu *et al.* [12].

This is an pre-print of the paper published by Elsevier in Applied Thermal Engineering 106 (2016) 1337–1344
kris@kubiak.co.uk
http://dx.doi.org/10.1016/j.applthermaleng.2016.06.128

3.3 Multi-design optimisation

Firstly, the design goal is formulated as the unconstrained, optimization problem of maximizing the jumping velocity $\bar{v}_j$. The global minimum of the surrogate model for $\bar{v}_j$ is obtained using a single-objective genetic algorithm (GA) approach. The parameters of the optimal design were obtained as follows: r=35μm, θ=161^0 with consequential jumping velocity $\bar{v}_j$=0.226m/s from the surrogate model. An illustrative example of surface functions $\bar{v}_j$ in terms of the design variables r and θ is shown in Figure 11.

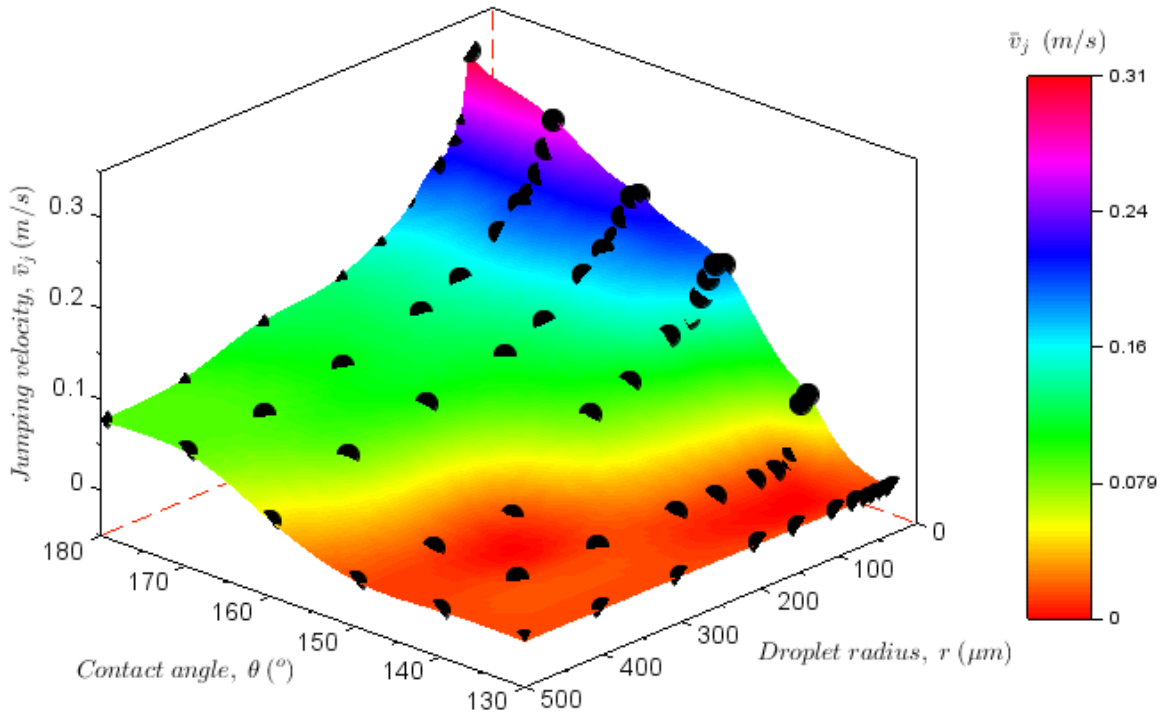

Figure 11: Response surface of the jumping velocity $\bar{v}_j$ from the surrogate model together with the DOE points; ●.

Table 1: Super-hydrophobic functional surface performance at stages of the single-objective design process.

	Response from	$\bar{v}_j$
Best design from DOE	LBM	0.314
Optimized design after GA	RBF	0.226
CFD prediction with optimized design variables	LBM	0.242
	VOF	0.216

The optimized design from the surrogate model was validated against our corresponding 2D LBM and 3D VOF CFD solutions with the same design variables. They showed good agreement with the surrogate model with $\bar{v}_j^{LBM}$ = 0.242m/s and $\bar{v}_j^{VOF}$ = 0.216m/s which are within 7% of the surrogate's prediction. The results of the validation process and the predicted functional surface performance objective function $\bar{v}_j$ for the single-objective function are given in Table 1 together with the best design from the DOE. Note that our GA algorithm restricted the parameter range for the optimization to a maximum contact angle of 170^0, which reflects the practical difficulties of obtaining a

This is an pre-print of the paper published by Elsevier in Applied Thermal Engineering 106 (2016) 1337–1344
kris@kubiak.co.uk
http://dx.doi.org/10.1016/j.applthermaleng.2016.06.128

physical system with a contact angle that is closer to 180^0. The best DOE result was actually achieved for a contact angle of 180^0 however, which leads to a theoretically higher value for the best possible jumping velocity.

Secondly, the design goal is now formulated as the unconstrained, multi-objective optimization problem of maximizing the jumping velocity $\bar{v}_j$ and q simultaneously. The global minimum of the surrogate model for $\bar{v}_j$ and q is obtained using a multi-objective genetic algorithm (GA) approach based on [32-33]. For the computation of q, ΔT=4 K, A=(500μm)^2, c_p=4200J/kgK and ρ_l=1000m^3/kg. The parameters of the optimal design were obtained as follows: r=39μm, θ=166^0 with resulting jumping velocity $\bar{v}_j$=0.228m/s from the surrogate model. An illustrative example of surface functions q in terms of the design variables r and θ is shown in Figure 12.

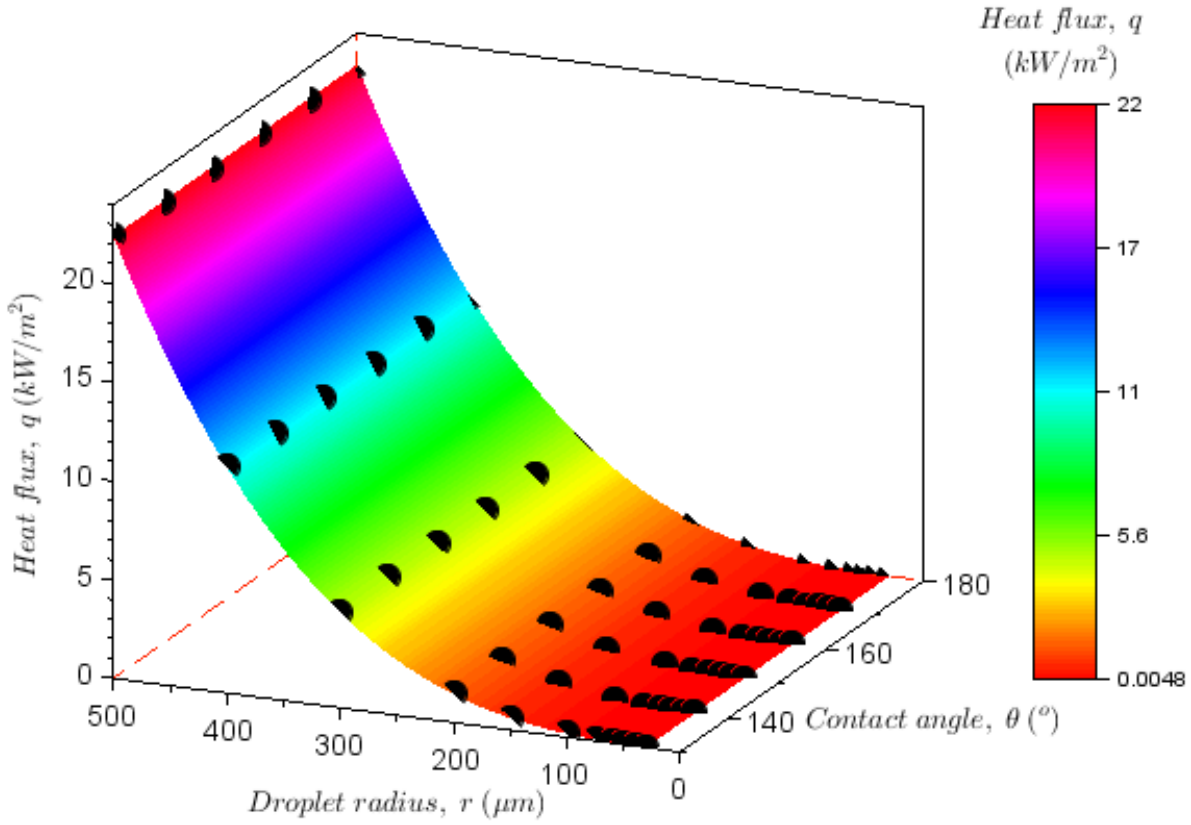

Figure 12: Response surface of the heat flux q together with the DOE points;●.

Table 2: Super-hydrophobic functional surface performance at stages of the multi-objective design process.

	Response from	$\bar{v}_j$	q
Best design from DOE	LBM	0.314	0.005
Optimized design after GA	RBF	0.228	0.015
CFD prediction with optimized design variables	LBM	0.246	0.011
	VOF	0.220	0.011

The optimized design from the surrogate models was validated against our corresponding 2D LBM and 3D VOF CFD solutions with the same design variables. They showed good agreement with the

This is an pre-print of the paper published by Elsevier in Applied Thermal Engineering 106 (2016) 1337–1344
kris@kubiak.co.uk
http://dx.doi.org/10.1016/j.applthermaleng.2016.06.128

surrogate model with $\bar{v}_j^{LBM}$ = 0.246m/s and $\bar{v}_j^{VOF}$ = 0.22m/s which are within 8% of the surrogate's prediction. The heat fluxes, $q^{LBM} = q^{VOF}$ = 0.011 kW/m^2. The results of the validation process and the predicted functional surface performance objective functions $\bar{v}_j$ and q for the multi-objective functions are given in Table 2 together with the best DOE design. Although this best DOE design again leads to a higher jumping velocity, the predicted heat flux is significantly lower than the optimal value in this case.

In a multi-objective optimisation problem a Pareto front can be used by designers to choose the most appropriate compromise between the various objective functions that have been identified and for which the goal is to minimise the objective functions. It is not possible to move along the design points on the Pareto front to decrease any of the objective functions without increasing at least one other objective function, and Pareto points are often referred to as being 'non-dominated'. In the present case with two objective functions the Pareto front showing the impact of the two objectives of interest here is shown in Figure 13. This data provides a convenient and scientifically-rigorous means by which designers can quantify the effect of their design criteria on both manufacturability and energy efficiency of functional surfaces.

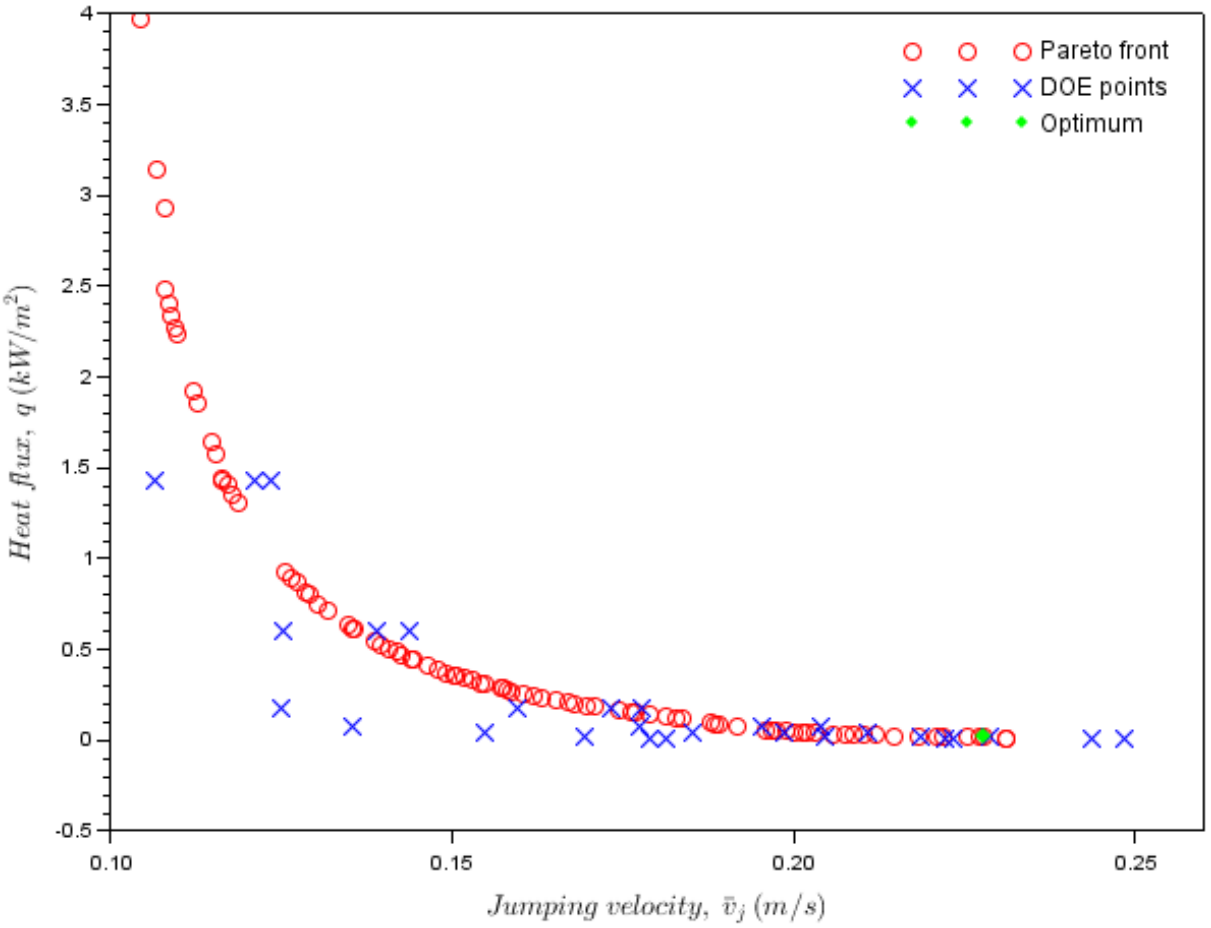

Figure 13: Pareto front showing the compromises that can be obtained in maximising both $\bar{v}_j$ and q.

4 Conclusions

Evacuation of condensate during dropwise condensation is technologically challenging. The process of droplet coalescence on superhydrophobic surface, and resulting jumping phenomenon, have been analysed experimentally and successfully modelled numerically with both 2D lattice Boltzmann and

This is an pre-print of the paper published by Elsevier in Applied Thermal Engineering 106 (2016) 1337–1344
kris@kubiak.co.uk
http://dx.doi.org/10.1016/j.applthermaleng.2016.06.128

3D Volume of Fluid techniques. The coalescence-induced velocity of jumping droplets has been explored, and optimal kinematic conditions for jumping droplets have been established to be in a range of initial droplet radii from r=20μm to 40μm, for a static contact angle in the proximity of θ_s~160º. Critical value of static contact angle for jumping phenomenon to take place has been found to be around θ_c~140º. It is clear that the development of functional surfaces to obtain continuous drop-wise condensation can be a good strategy to enhance the heat transfer rate in condensation processes. The heat transfer model used in this paper is, like many others in the literature (such as [13], for example), relatively simply: based upon an assumption that the heat transfer between the surface and the droplet occurs almost instantaneously. Future work should explicitly model thermal energy transfer within the fluid as the droplets coalesce in order to assess the range of validity of this assumption.

References

[1] Bhardwaj R., ten Kortenaar M.V. and Mudde R.F., Orientation effects of nanoparticle-modified surfaces with interlaced wettability on condensation heat transfer, *Applied Thermal Engineering*, 98, 2016, 480-490.

[2] Miljkovic N., Enright R., Nam Y., Lopez K., Dou N., Sack J. and Wang E.N., Jumping-Droplet-Enhanced Condensation on Scalable Superhydrophobic Nanostructured Surfaces, *Nano Lett.*, 13 (1), 2013, 179-187.

[3] Boreyko J.B and Chen C.H., Self-Propelled Dropwise Condensate on Superhydrophobic Surfaces, *Phys. Rev. Lett.*, 103, 2009, 184501.

[4] J.B. Boreyko J.B., Zhao Y.J. and Chen C.H., Planar jumping-drop thermal diodes, *Appl. Phys. Lett.* 99, 2011, 234105.

[5] Miljkovic N. and Wang E.N., Condensation heat transfer on superhydrophobic surfaces, *MRS Bull.* 38, 2013, 397–406.

[6] Miljkovic M., Enright R. and Wang E.N, Modeling and optimization of superhydrophobic condensation, *J. Heat Transfer* 135, 2013, 111004.

[7] Kim H. and Nam Y., Condensation heat transfer performance of nano-engineered Cu surfaces, *Journal of Physics: Conference Series* 557, 2014, 012109.

[8] Wang F.C., F. Yang F. and Zhao Y.P., Size effect on the coalescence-induced self-propelled droplet, *App. Phys. Lett.* 98, 2011, 053112.

[9] Peng B., Wang S., Lan Z., Xu W., Wen R and Ma X., Analysis of droplet jumping phenomenon with lattice Boltzmann simulation of droplet coalescence, *App. Phys. Lett.* 102, 2013, 151601.

[10] Nam Y.S., Kim H.S. and Shin S.W., Energy and hydrodynamic analysis of coalescence-induced jumping droplets, *Appl. Phys. Lett.* 103, 2013, 161601.

[11] Nam Y.S., Seo D.H., Lee C.Y. and Shin S.W., Droplet coalescence on water repellent surfaces, *Soft Matter* 11, 2015, 154.

[12] Liu F., G. Ghigliotti G., Feng J.J. and Chuan-Hua Chen, Numerical simulations of self-propelled jumping upon drop coalescence on non-wetting surfaces *J. Fluid Mech.* (2014), 752, pp.39-65.

[13] Cheng Y, Xu J. and Sui Y., Numerical investigation of coalescence-induced droplet jumping on superhydrophobic surfaces for efficient dropwise condensation heat transfer, *International Journal of Heat and Mass Transfer*, 95, 2016, 506–516.

[14] Shan X. and Chen H., Lattice Boltzmann model for simulating flows with multiple phases and components, *Phys. Rev. E* 47, 1993, 1815.

[15] Sukop M.C. and Thorne D.T., Lattice Boltzmann modeling: an introduction for geoscientists and engineers, 2005, Springer Berlin.

[16] OpenLBMflow, Open source lattice Boltzmann solver, website: http://www.lbmflow.com.

This is an pre-print of the paper published by Elsevier in Applied Thermal Engineering 106 (2016) 1337–1344
kris@kubiak.co.uk
http://dx.doi.org/10.1016/j.applthermaleng.2016.06.128

[17] Castrejon-Pita J.R., Kubiak K.J., Castrejon-Pita A.A., Wilson M.C.T and Hutchings I.M., Mixing and internal dynamics of droplets impacting and coalescing on a solid surface, *Phys. Rev. E* 88, 2013, 023023.
[18] Deshpande S.S., Anumolu L. and Trujillo M.F., Evaluating the performance of the two-phase flow solver InterFoam, *Comput. Sci. Disc.* 5, 2012, 014016.
[19] OpenFOAM, Free Open Source CFD, website: http://www.openfoam.org.
[20] Khatir Z. and Lucey A.D., A combined boundary integral and vortex method for the numerical study of three dimensional fluid flow systems', *Intern. J. of Computer Math*, Vol. 89/11, pp. 1504-1524, 2012.
[21] Hirt C.W. and Nichols B.D., Volume of fluid (VOF) method for the dynamics of free boundaries, *Journal of Computational Physics*, 1981, 39, 201-225.
[22] Guilizzoni M., Drop deposition and low-speed impact on flat, curved and microfinned solid surface: comparison between simulations, models and experiments", *DIPSI Workshop 2012 on Droplet Impact Phenomena & Spray Investigation*, May 18, 2012, Bergamo, Italy.
[23] Ubbink H., Computational Fluid Dynamics of Dispersed Two-Phase Flows at High Phase Fractions, *Ph.D Thesis*, Imperial College of Science, Technology and Medicine, London, 2002.
[24] Berberovic E., Van Hinsberg N.P., Jakirlic S., Roisman I.V. and Tropea C., Drop impact onto a liquid layer of finite thickness: Dynamics of the cavity evolution, *Physical Review*, 79, 2009.
[25] F. Raees, D.R. van der Heul, C. Vuik, Evaluation of the interface-capturing algorithm of OpenFOAM for the simulation of incompressible immiscible twophase flow, Report 11-07 ISSN 1389-6520, Reports of the Department of Applied Mathematical Analysis, Delft University, Netherlands, 2011.
[26] Khatir Z., Taherkhani A.R., Paton J.B., Thompson H.M., Kapur N. and Toropov V.V., Energy thermal management in commercial bread-baking using a multi-objective optimisation framework. *Applied Thermal Engineering* (80) 141-149, 2015.
[27] Khatir Z., Thompson H., Kapur N., Toropov V. and Paton J., Multi-objective Computational Fluid Dynamics (CFD) design optimisation in commercial bread-baking. *Applied Thermal Engineering* (60) 480-486, 2013
[28] Khatir Z, Paton J.B., Thompson H.M., Kapur N. and Toropov VV., Optimisation of the energy efficiency of bread-baking ovens using a combined experimental and computational approach, *Applied Energy* (112) 918-927, 2013.
[29] Bassi A., A Scilab radial basis function toolbox, *Master's thesis*, University of Padova, Italy, 2012.
[30] Khatir Z., Pozarlik A.K., Cooper R.K., Watterson J.W. and Kok J.B.W., Numerical study of coupled fluid structure interaction for combustion system, *Int. J. Numer. Meth. Fluids.* vol. 56, pp.1343-1949, 2008
[31] Khatir Z. and Kubiak K.J., CFD based optimisation of the superhydrophobic functional surface in dropwise condensation, *Proceedings of International Conference on the Analysis and Mathematical Applications in Engineering and Science* (AMAES 2014), 19 – 22 January 2014, Curtin University Sarawak, Miri, Malaysia. ISBN 978-983-44482-6-4
[32] Fonseca C. M. and Fleming P.J., Genetic algorithms for multi-objective optimization: Formulation discussion and generalization. *Proceedings of the 5th International Conference on Genetic Algorithms*, pages 416-423, San Francisco, CA, USA, 1993. Morgan Kaufmann Publishers Inc.
[33] Deb K., Agrawal S., Pratap A., and Meyarivan T., A fast elitist non dominated sorting genetic algorithm for multi-objective optimization: Nsga-ii. pages 849-858, Springer, 2000.